(This paper is a preprint of the final paper which was published in the IEEE Photonic Technology Letters, Vol. 7, p526-528, 1995)

Highly Compact Optical Waveguides With A Novel Pedestal Geometry

Apurva D. Chaudhari[1], Lawrence C. West[2*], Charles W. Roberts[2*], and Yicheng Lu[1]

1. Dept. of Electrical and Computer Engineering, Rutgers University, Piscataway, NJ 08855, (908) 445-3466

2. AT&T Bell Laboratories, Room 4G-518, Holmdel, NJ 07733, (908) 949-8715

* Currently at Integrated Photonic Systems, Inc. P.O. Box 717, Clarksburg, NJ 08510, (609) 259-1654, e-mail: lcw@intphsys.com

ABSTRACT

A structure with large refractive index ratio between waveguide and cladding materials can be fabricated with low scattering losses by using Ge on GaAs waveguides at 10 μm wavelengths. We demonstrate two types of ultra high confinement (UHC) dielectric waveguides using separate geometries: a ridge and a novel pedestal. Computer simulations using a time domain Finite Element Method and microwave-scale experiments are performed on both waveguide types. We show a waveguide thickness of 0.18 of the free-space wavelength or greater guide well-confined single-mode light for both geometries. Numerical and experimental values of the effective index agree to better than 0.5%.

The idea of integrating the optical components onto a single chip was first suggested by S. E. Miller [1]. In spite of the offered promise of high density integration of optical components, two-dimensional lateral connectivity to date has nowhere approached that of VLSI electronics. The obstacle has been the incapability of guiding light with strong dielectric confinement due to the rapid increase in scattering with dielectric ratio. The scattering increases as a square of the difference in dielectric constant between guide and cladding, requiring the dielectric constants to remain within 1% of each other for a typical waveguide [2]. This requirement has caused the thickness of a typical waveguide to be larger than the free-space wavelength [3]. The practical problem of scattering is solved by the use of mid-infrared light because the scattering losses drop with wavelength to the third power [4,5]. We present in this letter an analysis of the Ultra High Confinement (UHC) waveguides created with a high refractive index ratio between cladding and guide. Ultra High Confinement is defined here as confinement of light in a waveguide with an effective cross-section less than a tenth of a squared free-space wavelength or a resonator volume less than a cubic free-space wavelength. Because of the high confinement, a full vector mode analysis is essential for accuracy. A practical implementation of an UHC waveguide in the mid-infrared region uses Ge with refractive index 4.0 on GaAs with refractive index 3.27 [6]. The Ge waveguide can be deposited on top of GaAs substrate. Both the materials have excellent infrared and thermal properties and have almost perfect lattice matching. Any active material can be grown on the GaAs substrate before the Ge evaporation and interact with the strong fields at the Ge/GaAs boundary. An entirely new class of physical devices using the intersubband transition can be used for this mid-infrared interaction. The physical phenomena include lasing, modulation, detectors, second harmonic generation and other nonlinear interactions [7]. The waveguide geometries discussed here can scale to the near-infrared as lithography improves with the use of GaAs with refractive index 3.6 as the waveguide on AlAs with refractive index 2.9 instead of Ge/GaAs. Using the numerical analysis and microwave experiments we show that a large index ratio confines the light into a waveguide with dimensions a small fraction of the wavelength of light. We also present a novel, pedestal waveguide structure that is simple and easy to fabricate and which further enhances the confinement of light.

Figure 1(a) shows an outline of the cross-section of the ridge waveguide geometry along with the contour plot of the mode. The ratio of the waveguide width to thickness is taken to be 2 for this analysis. The waveguide structure has the dimensions of 1.75 μm × 3.5 μm for 10 μm wavelength using 0.8 μm resolution lithography. This lithography linewidth resolution is several times smaller than the actual waveguide width to assure sufficiently smooth waveguide edges and surface relative to the wavelength so as to minimize the scattering losses as discussed earlier. The dimensions used here can be scaled down to 0.175 μm × 0.35 μm with the use of near-infrared light when the photolithography resolution has advanced to 0.1 μm or less. Figure 1(b) shows a cross-section of the novel pedestal waveguide structure and a contour plot of the modes. The Ge waveguide dimensions are similar to the ridge structure, but the waveguide etching is continued deeper into the substrate to form a GaAs pedestal underneath the waveguide. The thickness and width of the pedestal are same as that of the waveguide. The novelty of the pedestal structure lies in its very compact dimensions as compared to the free-space wavelength, its use of high index ratio unlike the rib waveguides, its ability to improve the lateral confinement of the fields within the waveguide as well as the substrate, and its ability to incorporate active materials at the interface to create devices. Mode confinement for both the structures are studied using computer simulations by a full 3D vector finite element method and the results are verified using microwave experiments performed on the scaled waveguide models having dimensions 1.27 cm × 2.54 cm in the microwave region.

Numerical modeling of the waveguides is performed using EMFlex, a 3D vector finite element method program in the time domain to compute the Maxwell's wave equation [8]. Time-domain analysis is performed on the models outlined in figures 1(a) and 1(b) by allowing 3D vector field propagation through it and using the radiation boundary conditions. An analytic mode [9] is injected on one edge of a scaled 1.5 μm × 3.0 μm Ge waveguide and propagated approximately 40 μm through the guide until reaching a steady state solution as higher order modes (about 10 to 20 percent of power of the original input mode) radiate away. Both ridge and pedestal waveguide structures are evaluated using the same procedure. The wavelength of the light is varied from 8 μm to 10 μm to study the mode confinement at various ratios of wavelength to waveguide dimension. Figures 1(a) and 1(b) show contour plots of the computer derived vertical mode component propagating through both types of the waveguides at wavelength of 8.43 μm. Note that in Figure 1 the pedestal waveguide provides better confinement than the ridge waveguide with more rounded beam and less spread into the substrate. Effective indices for both the waveguides are deduced from the time domain analysis at various wavelengths and plotted in Figure 3.

The experiment setup is shown in Figure 2. All the experiments are conducted inside a wooden microwave chamber (6.0' × 3.0' × 2.0'). Its inner walls are covered with microwave absorbing cones to reduce reflections off the walls. A slot (1.0'× 6.0') is cut in the top wall in order to suspend a half-wave dipole antenna into the chamber. The antenna can be moved to any location inside the chamber using motor-driven sliders along Y and Z directions and using manual adjustments along the vertical X direction. Stycast materials with refractive indices 4.0 and 3.27 are used to accurately model Ge and GaAs, respectively. A microwave signal is injected into the waveguide using coaxial-to-waveguide coupler via a 20 dB microwave amplifier. The front end of the high-index waveguide is slightly inserted into hollow opening of the coupler which essentially acts as a cavity whose three walls are metallic and one wall is a dielectric. X (TM) and Y (TE) polarization of the electric field vector are measured by pointing the dipole antenna at the opening of the coupler. The TM/TE ratio is found to be about 24 dB, assuring mostly the TM modes are transmitted into the waveguide. Along with the desired mode many higher order modes may also be coupled into the waveguide. Therefore, the first 100 cm of the waveguide is covered on all sides with microwave absorbing material, as shown in Figure 2, to absorb the high-order modes that are strongly radiative for our waveguide geometry. The bottom of the 10 cm thick substrate is also covered with an index matching absorber to remove radiation modes that leak into the substrate and would otherwise make multiple bounces by total internal reflection. Signal propagation through the waveguide is detected and measured by placing an antenna within 1 mm of the surface of the waveguide. After all the adjustments a clean single-mode injection is achieved with the noise and other extraneous microwave interference levels suppressed 20 dB below the waveguide signal. Measured amplitude variations of less than one dB as a function of propagation distance infers that the total interfering power in other modes is at the -20 dB level. The experiments are performed at various wavelengths ranging from 6.81 cm to 7.90 cm. The effective index is measured at each wavelength using linear least-squares fit on the phase oscillations. The resulting plot of the effective index versus the thickness over wavelength of the waveguide is shown in Figure 3. We find that for both types of structures, the confinement occurs for thickness $h > \lambda_0/6$, where λ_0 is the free-space wavelength. However, the pedestal waveguide guides the single-mode signal with the effective index as high as 3.41 compared to 3.35 for the ridge waveguide. The effective indices are also calculated for both the structures using an analytical semi-vectorial Spectral Index Method (SIM) [10]. The SIM modifies the original boundary around the ridge section by the polarization dependent evanescent boundary such that the field is zero outside the modified boundary. The scalar slab-like confined mode solution in the ridge section is used as the trial function to calculate the spectral mode solution inside the substrate region. The two solutions are matched at the ridge-substrate interface using the variational principle to give the transcendental eigenvalue equation. The effective indices calculated from this eigenvalue equation are plotted in Figure 3 to compare with the finite element method and the microwave experiment.

In conclusion, we show the ability to create highly compact waveguides using high index semiconductors to guide tightly confined single-mode light. We also show that the pedestal waveguide geometry improves the level of confinement. We find good confinement of light in a ridge waveguide with a thickness of around 17% of the free space wavelength and in a pedestal waveguide with a thickness of around 18%. The deviations in the numerical and the experimental effective index for the ridge and the pedestal waveguide structures are 0.31% and 0.30%, respectively. The deviation in the theoretical and the numerical effective index for the ridge waveguide is 0.33%, while for the pedestal waveguide it is 0.72%. Similarly, the theoretical and the experimental results deviate by 0.44% and 0.97% for the ridge and pedestal structures, respectively. We have used the pedestal geometry to create tight 90% efficiency optical bends with the radii of curvature less than the free-space wavelength. This result will be published in the future. Such a tight bend can dramatically decrease the chip area required to change the waveguide directions. This can allow the density of components in an optical integrated chip to be increased nearly to that of VLSI electronics for the creation of Very Large Scale Integrated Optics (VLSIO).

REFERENCE

[1] S. E. Miller, "Integrated optics: An Introduction," *Bell Syst. Tech. J.*, vol. 48, pp. 2059-2069, 1969.

[2] R. J. Deri, and E. Kapon, "Low-Loss III-V Semiconductor Optical Waveguides," *IEEE J. Quantum Electron.*, vol. 27, pp. 626-640, 1991.

[3] H. Kogelnik, "Limits in Integrated Optics," *Proc. IEEE*, vol. 69, no. 2, p. 232, 1981.

[4] D. Marcuse, "Mode Conversion Caused by Surface Imperfections of a Dielectric Slab Waveguide," *Bell Syst. Tech. J.*, vol. 48, pp. 3187-3215, 1969.

[5] D. Marcuse, "Radiation Losses of Dielectric Waveguides in Terms of the Power Spectrum of the Wall Distortion Function," *Bell Syst. Tech. J.*, vol. 48, pp. 3233-3242, 1969.

[6] M. Dubey, G. F. McLane, K. A. Jones, R. T. Lareau, D. W. Eckart, W. Y. Han, C. W. Roberts, J. P. Dunkel, and L. C. West, "Ge Optical Interconnects on a GaAs Surface," *MRS Proceedings*, vol. 340, p. 411, 1994.

[7] H. C. Liu, B. F. Levine, and J. Y. Andersson (eds.), *Quantum Well Intersubband Transition Physics and Devices*, Kluwer Academic Publishers, Netherlands, 1994.

[8] G. Wojcik, J. Mould, Jr., and L. C. West, "Time-Domain Finite Element Modeling of 3D Integrated Optical Devices," *Integrated Photonics Research Tech. Digest, W.D.1. Optical Society of America, eds.*, pp. 112-115, 1993.

[9] E. A. J. Marcatili, "Dielectric Rectangular Waveguide and Directional Coupler for Integrated Optics," *Bell Syst. Tech. J.*, vol. 48, pp. 2071-2102, 1969.

[10] P. N. Robson, and P. C. Kendall (ed.), *Rib Waveguide Theory by the Spectral Index Method*, New York: Wiley, 1990.

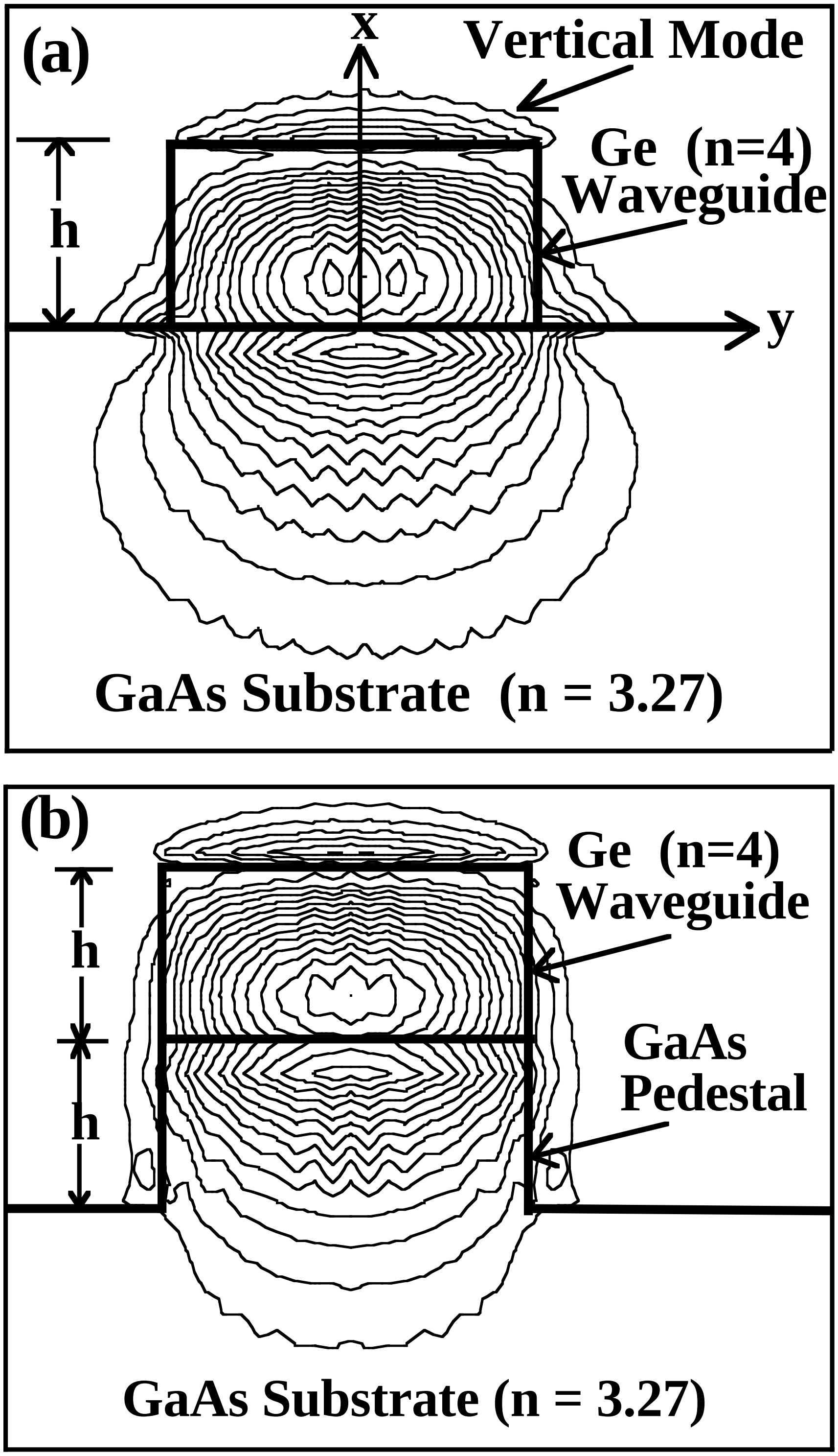

Figure 1: Vertical electrical field component of the vector mode profile deduced from the finite element method time domain analysis for a wavelength of 8.43 μm in (a) a ridge waveguide and (b) a pedestal waveguide. The waveguide structures are outlined by thick lines. The index of guide is 4.0 and the index of the pedestal and substrate is 3.27. As shown in (a), a large portion of the mode extends into the substrate; however, in (b) the mode penetration into the substrate is dramatically reduced by raising the waveguide above the substrate using a pedestal.

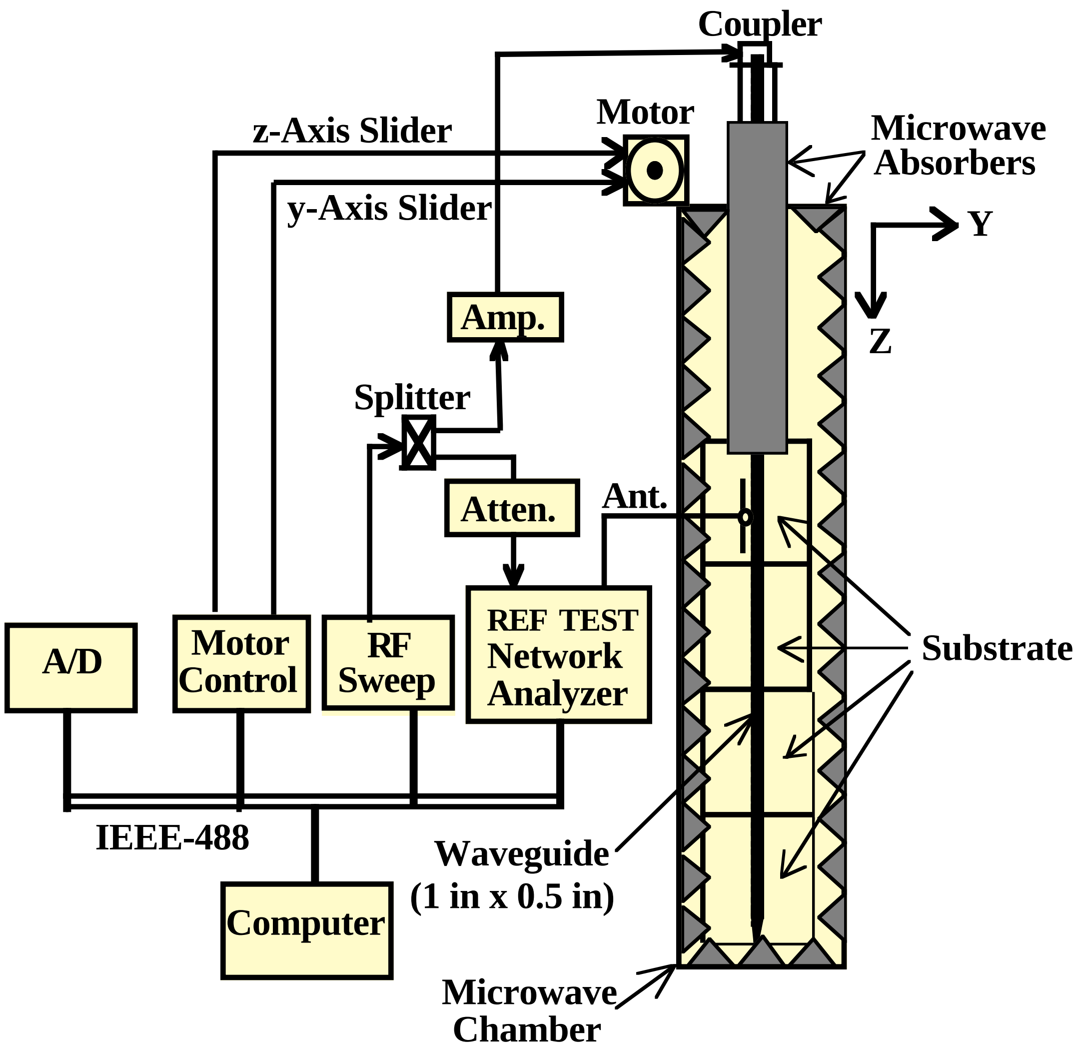

Figure 2: Plot of microwave experiment setup. Microwave signal is injected into the chamber through the coupler. *z-axis slider* and *y-axis slider* lines are connected to the motor driven sliders on which antenna is mounted. An antenna polarized along z axis is also shown in the figure. The antenna output is connected to the vector network analyzer.

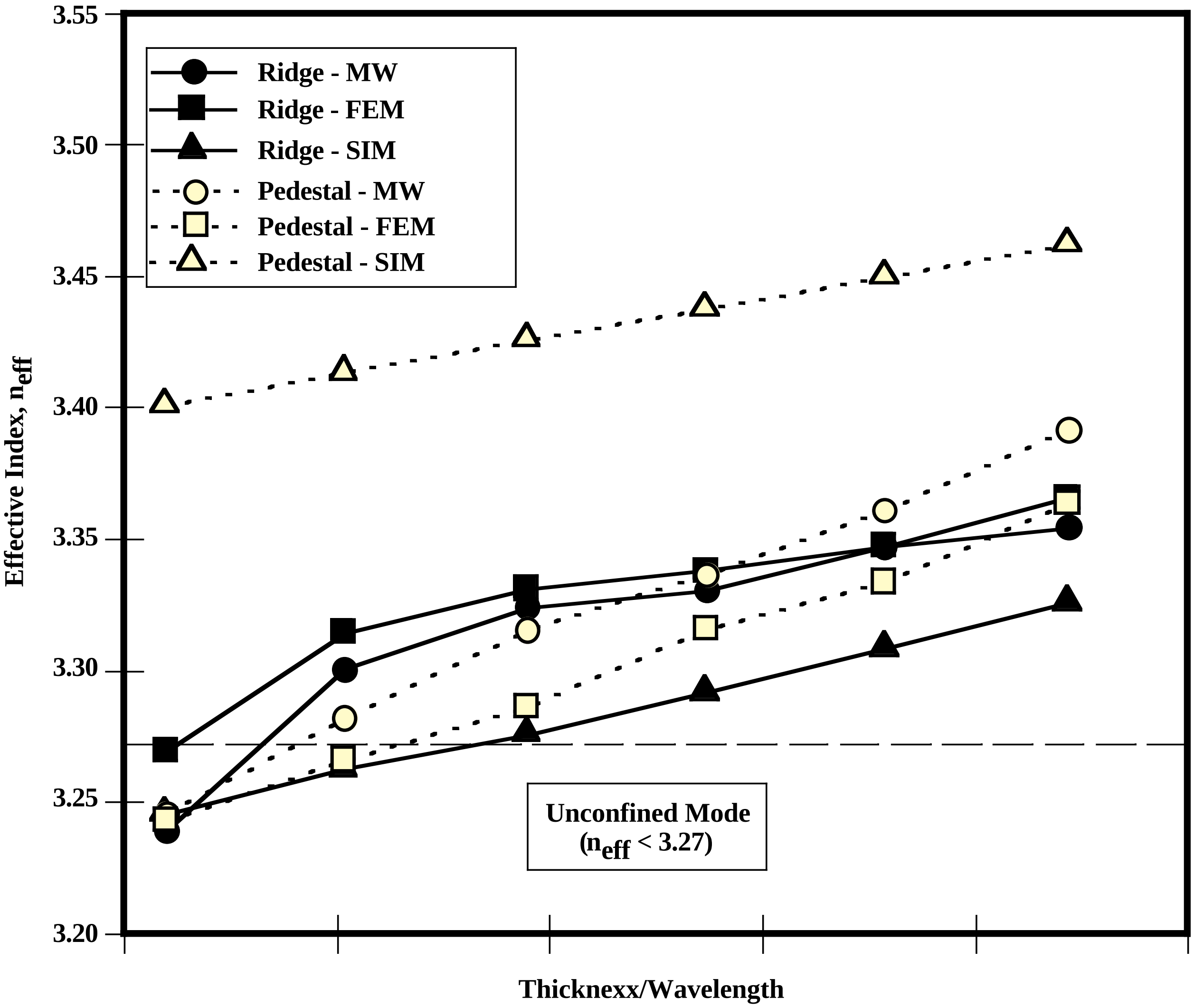

Figure 3: Effective index is plotted versus thickness/wavelength ratio of the waveguides. Dashed line shows the cutoff boundary below which the mode becomes radiative. Theoretical effective index plot is based on the spectral index theory [10]. For both types of waveguides, the thickness of $\lambda_0/6$ is sufficient to guide well-confined single-mode signal.